


RESEARCH

Open Access



Nanoparticles engineered to bind cellular motors for efficient delivery

Inmaculada Dalmau-Mena¹, Pablo del Pino^{2,3}, Beatriz Pelaz^{2,3}, Miguel Ángel Cuesta-Geijo¹, Inmaculada Galindo¹, María Moros², Jesús M. de la Fuente⁴ and Covadonga Alonso^{1*} 

Abstract

Background: Dynein is a cytoskeletal molecular motor protein that transports cellular cargoes along microtubules. Biomimetic synthetic peptides designed to bind dynein have been shown to acquire dynamic properties such as cell accumulation and active intra- and inter-cellular motion through cell-to-cell contacts and projections to distant cells. On the basis of these properties dynein-binding peptides could be used to functionalize nanoparticles for drug delivery applications.

Results: Here, we show that gold nanoparticles modified with dynein-binding delivery sequences become mobile, powered by molecular motor proteins. Modified nanoparticles showed dynamic properties, such as travelling the cytosol, crossing intracellular barriers and shuttling the nuclear membrane. Furthermore, nanoparticles were transported from one cell to another through cell-to-cell contacts and quickly spread to distant cells through cell projections.

Conclusions: The capacity of these motor-bound nanoparticles to spread to many cells and increasing cellular retention, thus avoiding losses and allowing lower dosage, could make them candidate carriers for drug delivery.

Keywords: Nanoparticles, Biomimetic synthetic peptides, Drug delivery, Microtubule motors, Dynein

Background

Motor proteins are biological molecules that transform chemical energy into mechanical force at the nanoscale [1]. These molecular motors can be integrated into hybrid biological and synthetic systems to functionalize nanoparticles (NPs) for biotechnological applications [2].

Engineered nanocomposites have been built in order to overcome intracellular barriers and to mimic how intracellular pathogens such as viruses transfer their genetic material into the cells [3]. Several design strategies have been tested in order to increase NPs translocation through cellular membranes, thereby enhancing transfection efficiency. Ligands conjugated to the surface of engineered NPs such as sugars [4] can influence the mode of cellular internalization [5]. Nevertheless, NPs of the same

composition may use alternative mechanisms for cell entry in different cell types [6].

Once inside the cell and given the crowded gel-like composition of the cytoplasm, the movement of organelles and macromolecules is restricted [7]. Furthermore, eukaryotic cells are compartmentalized by endomembrane systems and cytoskeleton filaments of actin, and microtubules are used as tracks for transport. This transport relies on energy-dependent molecular motors that are necessary for communication between compartments. To move in a crowded cellular environment poses problems to NP displacement and thus, vector design strategies have included different mediators of intracellular trafficking in order to facilitate this transport, some of them considering the cytoskeleton [8–10]. In fact, viruses, strictly depending on their capacity to invade and control the intracellular environment, have developed specific strategies to bind microtubule motors to facilitate their transport along these filaments to reach the perinuclear area and initiate replication [11–15]. Microtubule motor binding is crucial for the replication

*Correspondence: calonso@inia.es

¹ Dpt. Biotecnología, Instituto Nacional de Investigación y Tecnología Agraria y Alimentaria (INIA), Carretera de la Coruña km 7.5, 28040 Madrid, Spain

Full list of author information is available at the end of the article

and dissemination of several viruses. In-depth knowledge of some of these strategies of virus-cell interaction can be exploited to design virus-free delivery systems [16–18].

We used a biomimetic approach based on selected peptide sequences from viral proteins known to bind dynein. Dynein is a microtubule motor acting as a hub protein within the microtubule-motor complex, which exerts several functions related to movement in mammalian cells. This protein is responsible for cargo transport within cells, up to organelle-size cargoes [19]. It is also responsible of nuclear positioning within the cell and has several functions in mitosis [20–22]. Onset of mitosis is marked by centrosome migration for the mitotic spindle formation that requires dynein. Also, dynein action on microtubules leads to nuclear envelope breakdown at early mitosis and to its reorganization after the end of cell division [23–25]. The loss of nuclear compartmentalization induced by the breakdown of the nuclear envelope is characterized by increased permeability together with the initiation of the nuclear pore disassembly [26]. Thus, dynein has the potential capability to drive nuclear envelope disassembly and permeate this layer, that is, a particularly important property since the nuclear membrane is the “last barrier” for gene delivery in non-dividing cells.

Dynein exists within a complex of several subunits and adaptors [27] and contains two heavy chains and several intermediate, light intermediate and light chains [28, 29]. One of the light chains is DYNLL1, a highly evolutionarily conserved protein that is hijacked by a number of viral proteins for transport [30]. The high affinity interaction of viral proteins with DYNLL1 [31] and its ability to form long half-live molecular complexes make this molecule especially appropriate to build supramolecular structures [32]. Then, we used peptide sequences from viral proteins interacting with DYNLL1 to modify NPs based in the hypothesis that this modification could confer dynamic properties to the NPs, enhancing their motility and dispersion in the intracellular environment.

In the present work, gold NPs (Au NPs) have been modified with short peptide sequences taken from viral proteins that bind dynein. We found a highly active intracellular trafficking and cellular uptake of those modified carriers in several cell lines. Dynein-binding peptides (DBPs) modified NPs were motile throughout the cytosol and travelled from cell-to-cell favoring the propagation of this uptake. By this active cellular transport, NPs acquired the property to shuttle the nuclear membrane in non-dividing cells.

Results

Dynein-binding peptides modified nanoparticles design

Here, we report the production of water-soluble and stable Au NPs modified with DBPs as an efficient approach

for cargo delivery. Au NPs of different sizes have been widely used because of lack of apparent toxicity, and easy elimination by renal clearance in case NPs are small enough (sizes below 10 nm) [33, 34]. Coating NPs with organic molecules and/or macromolecules has been typically employed in order to improve NP stability and prevent aggregation [33], as for instance Au NPs coated with tiopronin (Au@tiopronin) [35]. Tiopronin is a thiolated derivative of the amino acid glycine. Au@tiopronin were prepared using the procedure originally reported by Murray et al. [34]. These NPs consist of small (typically, core diameter < 3 nm) Au NPs stabilized with the non-natural amino acid tiopronin (*N*-2-mercaptopropionylglycine), which has a free terminal carboxyl group, allowing to functionalize Au@tiopronin with aminated molecules [35], such as the DBPs sequences, by carbodiimide chemistry, *cf.* Figure 1. The reaction was executed in a methanolic/acetic acid mixture, dissolving HAuCl₄ and tiopronin to give a stable solution. The addition of NaBH₄ as reducing agent provided a dark solution by reduction of the gold salt and formation of the NPs. Acidic conditions are very important to guarantee the protonation of tiopronin carboxylic groups, and provide an efficient and dense self-assembled monolayer of tiopronin onto the NPs. The obtained NPs were colloidal stable in aqueous solution. The excess of tiopronin and salts was eliminated by dialysis. The purified NPs were characterized by TEM and UV/Vis, *cf.* Additional file 1: Figure S1. TEM images showed a mean diameter of 2.8 nm for the Au core (Fig. 1a). The UV/Vis absorption spectra showed an almost non-detectable surface plasmon band consistent with the small NP size of the NPs, *cf.* Additional file 1: Figure S1.

Using the reactivity of the tiopronin carboxylic group, further functionalization with aminated molecules was carried out using a procedure previously described [35] (Fig. 1): 1) Aminated poly(ethylene glycol) (PEG) derivative (CH₃O-PEG-NH₂); 2) different peptide sequences (Table 1) and 3) fluorescent dye TAMRA-CAD (*i.e.*, tetramethylrhodamine 5-carboxamide cadaverine), which was used to optimize carbodiimide coupling conditions. PEG molecules were selected to avoid unspecific interactions. A dense layer of PEG confers anti-fouling properties to nanomaterials, thereby increasing their colloidal stability in aqueous solution and reducing unspecific interactions with other molecules such as plasma proteins [36–38].

The selected dynein-binding peptide (DBP) sequences were synthetic peptides spanning the dynein-binding domain of different proteins, *cf.* Table 1. We selected three peptides: DynPro (dynein-propelled) derived from the product of the E183L gene of the African swine fever virus (p54) [11, 31]; ShortPro, a shorter sequence of the same protein based on the critical amino acids for

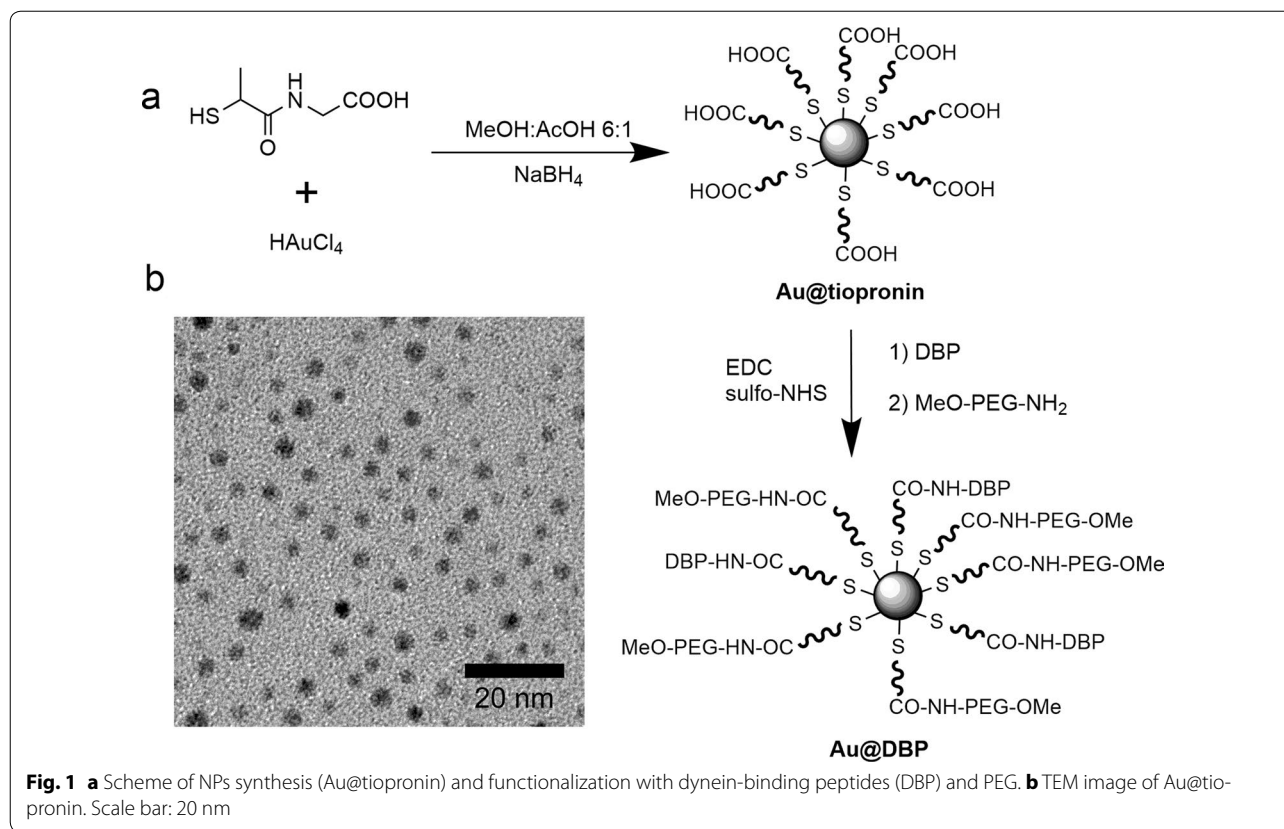


Fig. 1 a Scheme of NPs synthesis (Au@tiopronin) and functionalization with dynein-binding peptides (DBP) and PEG. b TEM image of Au@tiopronin. Scale bar: 20 nm

Table 1 Alias, sequence and molecular weight (MW) of the peptides used to surface modify the Au@tiopronin NPs

Alias	Amino acid sequence	MW (Da)
DynPro	GGGGK(TAMRA)-HPAEPGSTVTTQNTASQTMS-RRRRRRRR	4063.5
ShortPro	GGGGGGGGK(TAMRA)-YTTQNTASQTMS-RRRRRRRR	3578.9
TrasnRb	GGGGGGGGK(TAMRA)-FPNPSGRSSEDKSTQTAG-RRRRRRRR	4112.5
IntCt	GGGGK(TAMRA)-SLVSSDESVLHGSHESGEHV-RRRRRRRR	4110.5

dynein-binding; and TransRb derived from the Rabies virus P protein [39]. As a negative control, a non-dynein-binding amino acid sequence (IntCt) was selected. To guarantee the proper presentation of the peptides and minimize steric hindrance due to a dense packaging of molecules on the NP surface, a tetra- or octa-glycine tail was added to DynPro and IntCt, or ShortPro and TransRb, respectively. After the glycine-tail, a lysine residue was added. Primary amine moieties of the lysine residues were used for fluorescent labeling with 5-carboxytetramethylrhodamine (TAMRA). Finally, an octa-arginine tail was added to these peptides' end, including to the

control peptide IntCt, to increase the positive charge of the peptides, thereby enhancing cellular uptake, cf. Table 1.

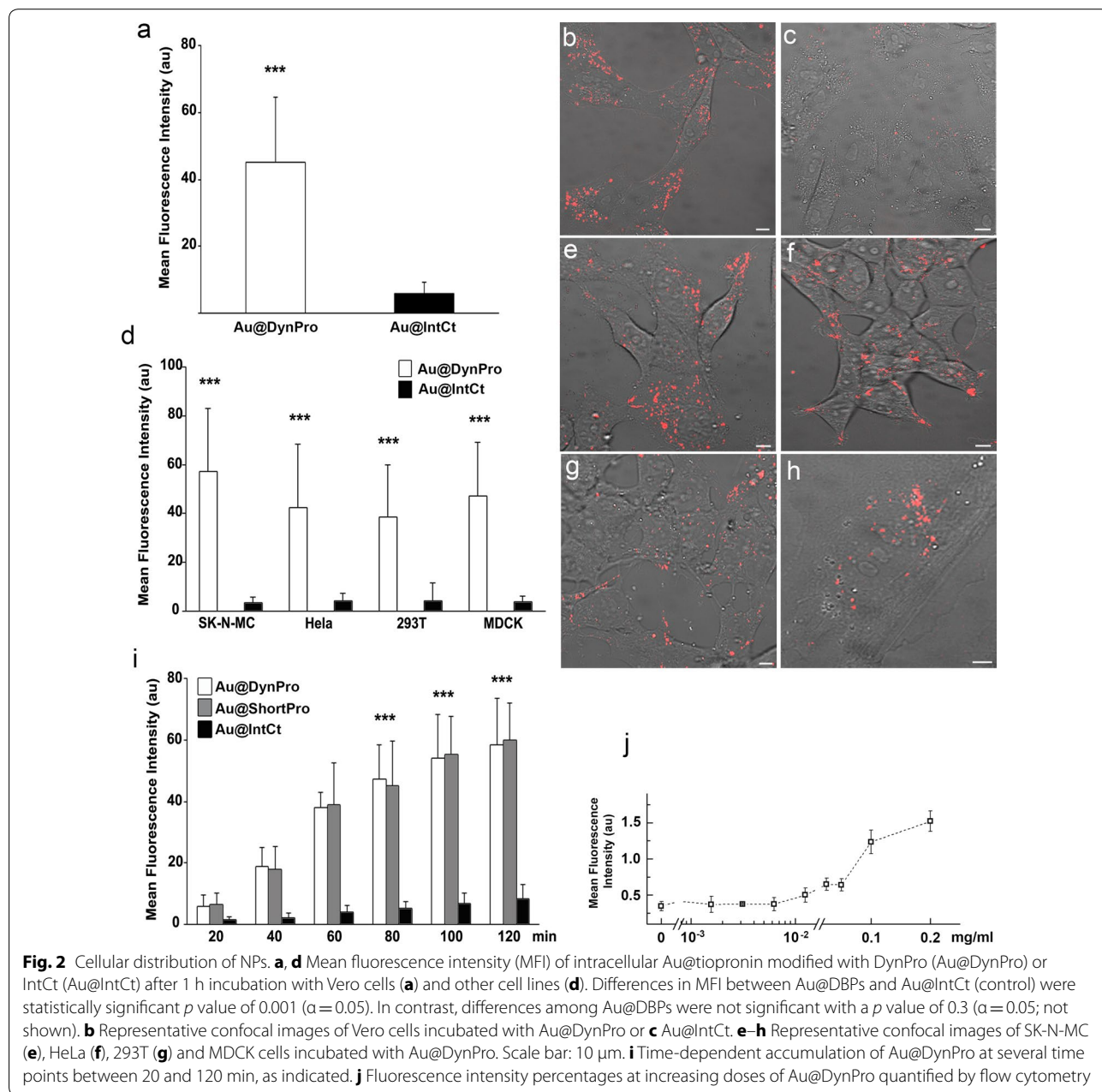
NPs' carboxyl groups and primary amines of the selected ligands (PEG derivative, TAMRA-CAD and DBPs) were crosslinked with the water-soluble carbodiimide N-[3-(dimethylamino)propyl]-N'-ethylcarbodiimide hydrochloride (EDC). N-hydroxysulfosuccinimide (sulfo-NHS) was also included in the reaction mixture to improve the efficiency of the carbodiimide-mediated amide-forming reaction by producing hydrolysis-resistant active ester reaction intermediates (Fig. 1). The resultant library of NPs was analyzed by ζ-potential, UV/Vis and fluorescence spectroscopy, probing that the molecules were incorporated to the NPs and the absence of aggregation after peptide coupling, cf. Additional file 1: Figure S3.

Modified nanoparticles internalization

NPs covalently functionalized with TAMRA-labeled peptides were visualized by live-cell imaging, which allowed tracking of their movement at the intracellular level. The cellular uptake of Au@tiopronin NPs modified with DBPs (Au@DBPs; Fig. 2b, e–h) was significantly more efficient compared to those functionalized with the control

peptide IntCt (*i.e.*, Au@IntCt) in Vero cells ($p < 0.001$; Fig. 2c). Similar results were obtained with other cell lines, such as the neuroblastoma cell line SK-N-MC, the epithelial cell line MDCK, HeLa (derived from a human epithelial carcinoma) and HEK293T cell line (human kidney embryonic transformed cell line; Fig. 2d–h). Time-dependent intracellular accumulation was observed from 20 to 120 min with Au@DBPs and Au@IntCt (Fig. 2i). Concentration of Au@DBPs increased until 180 min, remaining stable thereafter and visible up to 12 h.

Quantitative fluorescence percentages were also analyzed by flow cytometry with increasing doses of NPs (Fig. 2j). Overall, the cellular distribution among the functionalized Au@DBPs was similar (Fig. 3a–c). Au@DBPs were rapidly internalized and distributed widely within the cell and throughout the culture. While NPs stability in cell culture media was clearly observed, PEG modification did not result in significant modification of Au@DBPs uptake in cells incubated with 0.2 mg/ml NPs (*ca.* 1.5 μM NPs) for several times 1, 2 or 3 h (Additional file 1: Figure S4).



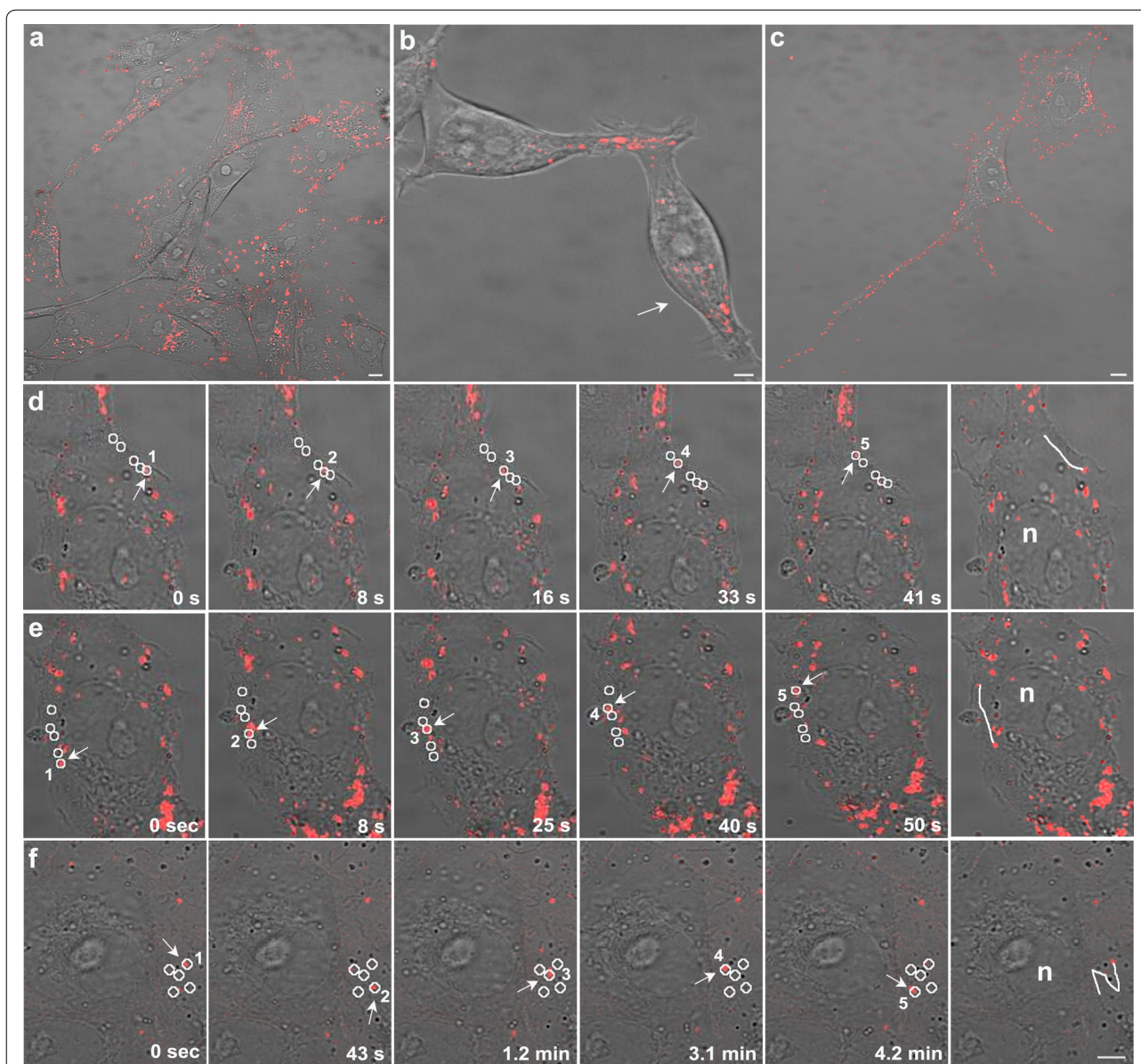


Fig. 3 Representative confocal images at low magnification of **a** Vero cells with Au@DynPro **b** HEK293T cells with Au@ShortPro and **c** MDCK cells with Au@TransRb. Representative images showed similar NP dispersion throughout the culture and cell-to-cell transfer of Au@DynPro through short (**b**) or long (**c**) projections. **d, e** Representative time-lapse images of the linear progression of Au@DBP inside the cell and the resulting trajectories (circles). **f** Comparison with the non-linear movement obtained with control NPs Au@IntCt. Scale bar: 5 μm

Nanoparticles dynamic properties

Time-lapse videomicroscopy unraveled Au@DBP bidirectional movement across the cytosol and a continuous flow to cell projections reaching neighboring or distant cells (Fig. 3a-c and Additional file 2: Movie 1). Also, we observed bidirectional movement towards the cell periphery, to cell projections and intercellular cell-to-cell transport. No differences were found among Au@DBPs in terms of distribution and dynamic properties (Fig. 3a-c, Additional file 2: Movies 1, Additional file 3: Movies 2).

Au@DBPs exhibited high-speed mobility (median speed $0.25 \pm 0.2 \mu\text{m/s}$). This movement followed linear trajectories allowing progression of Au@DBPs (Fig. 3d, e). In contrast, the movement of NPs functionalized with control peptide (Au@IntCt) was non-progressive, non-linear (Fig. 3f).

Microtubule-dependent transport of nanoparticles

Linear movement of Au@DBPs, with occasional pauses and alternating directions, suggested that this was a

microtubule-dependent transport. During the first minutes after incubation, Au@DBPs were rapidly internalized, moved and accumulated near the nucleus at the microtubule-organizing center (MTOC) (Fig. 4a). This preferential localization of Au@DBPs at the MTOC

was found in non-polarized cells (Fig. 4b). Conversely, in polarized cells, movement was directed to the cell periphery and to cell projections (Fig. 4c). Linear movement of Au@DBPs was bidirectional, reached the cell periphery and projections being transported from one

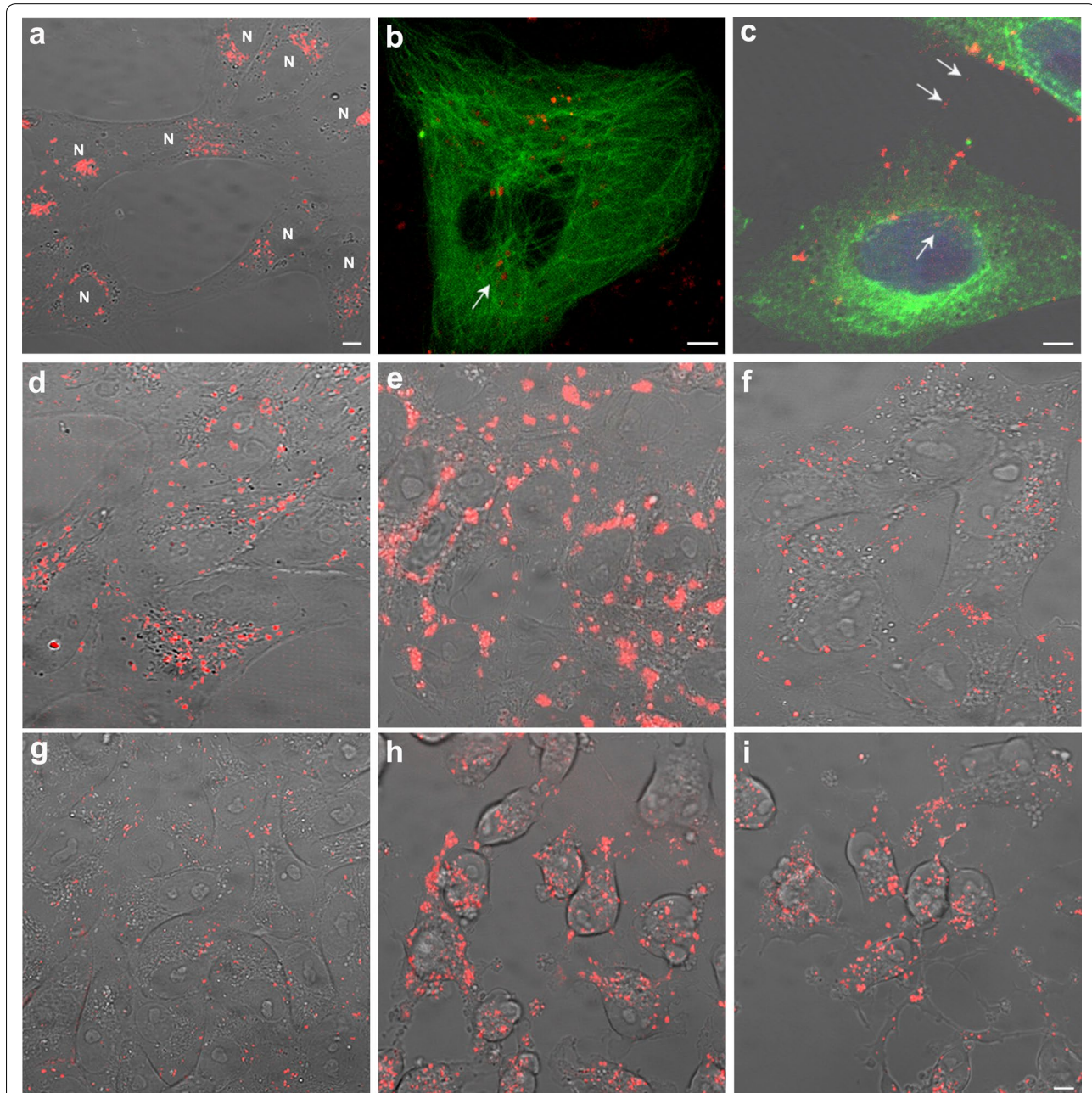


Fig. 4 **a** Accumulation of Au@DynPro at the MTOC near the nucleus (N). **b** Progression of Au@DynPro towards the MTOC, or **c** nucleus and projections (arrows) in GFP-tubulin transfected cells. **d–i** Au@DynPro's mobility was sensitive to microtubule-depolymerizing drugs. **d, g** Widespread cellular distribution of Au@DynPro before depolymerizing drug treatment, **e** Au@DynPro transport blockade and accumulation after 1 h drug incubation with 2.5 μM Nocodazole, and **f** mobility and dispersion recovery after washing. **g** Vero cells treated with 10 μM Au@DynPro and then **h** incubated for 1 h with 0.1 μM actin depolymerizing-drug LatrunculinA. This drug produced cell shrinkage because of actin cytoskeleton collapse that was not recovered after washing (**i**). However, Au@DynPro transport was still preserved within cells and projections. Scale bar: 10 μm

cell to another. These characteristics were found for all Au@DBPs tested.

Au@DBP dispersed distribution, movement and spread (Fig. 4d) was reversibly stopped with the microtubule depolymerizing agent Nocodazole (Fig. 4e). After washing and media replacement, movement and dispersion of Au@DBPs in the culture were recovered (Fig. 4f). In contrast, drugs that depolymerize the actin cytoskeleton, such as Latrunculin A, did not stop the motion of the Au@DBP between cells through projections, even under conditions of cell collapse after actin cytoskeleton depolymerization (Fig. 4g–i). This effect was not reversible by washing and media replacement as expected.

Efficient transport of Au@DBP across the nuclear membrane

Au@DBPs crossed the nuclear envelope and travelled the nuclear compartment (Fig. 5). This property was found for all the different Au@DBPs tested but not for the control Au@IntCt (Fig. 2c). Au@DBPs produced a visible imprint of their movement along the nucleus that was physically evident using bright field microscopy as linear protrusions as Au@DBPs moved through the nuclear area and the nucleolus (Fig. 5a, b, g).

Au@DBPs travelled across the nuclear envelope and the nuclear lamina, as shown in GFP-laminB receptor (Fig. 5c) and GFP-laminB1 transfected cells (Fig. 5d, e). In fact, Au@DBPs produced invaginations of the nuclear envelope at multiple sites (Figure 5c–e).

In the nucleolus, peptides colocalized with GFP-B23 nucleolin as they crossed the nucleolus, without affecting the morphology of this structure (Fig. 5f). Similarly, Au@DBPs entered nucleolus (Fig. 5g).

It is important to note that cell viability and cell proliferation were unaffected with any Au@DBP formulation (Additional file 1: Figure S5).

Discussion

Molecular motors have previously allowed developing nanoscale transport systems powered by biomolecular motors or molecular shuttles [7]. Peptides binding to a cellular protein that is highly evolutionarily conserved (DYNLL1) [19] and a molecular hub building long-life molecular complexes in cells, made this transport very efficient in a number of cell lines tested, including mammalian cells and some of non-mammalian origin [21, 27, 40].

Here, the dynamic properties of DBPs were successfully translated into Au NPs (*i.e.*, Au@DBPs), which may be highly useful in the drug delivery area. These results are in agreement with previous reports that employed soft carriers, such as microspheres [41] or liposomes [42], functionalized with dynein light chain 8 (LC8) peptide

binding motifs. Similarly, in the present work, we selected peptides able to bind a dynein chain with very high affinity [31], which were linked to hard Au@tiopronin NPs. In our study, non-significant differences regarding dynamic properties between Au@DBPs and “bare” DBPs were observed. Probably, this fact occurs due to the small size of our Au NPs, limiting the interaction of one dynein with one NP. Moreover, a previous theoretical work suggested that motor protein binding molecules attached to solid carriers work collectively rather than cooperatively [43].

NPs are small particles (from a few to 200 nm in diameter) especially useful for delivery as can be aerosolized [44], can be made highly biocompatible, allow site specific targeting to a specific cell population, permit controlled drug release and can be designed to biodegrade in an acceptable time span [35, 45]. The stability found for Au@DBPs and long times of persistence inside the cultured cells, make them suitable candidates for drug delivery. The Au@DBPs ability for spreading to neighboring cells remaining intracellular would improve efficacy and optimize dosage for compounds to be delivered.

Dynein has a central role in the formation of the mitotic spindle during mitosis and interacts dynamically with the nuclear envelope directing assembly and reassembly of nuclear lamins. The penetration capacity of Au@DBPs could rely on the ability of dynein to interact dynamically with the nuclear envelope and thus direct the disassembly of nuclear lamins as it occurs at early stages of mitosis [23, 25]. Other cell delivery mechanisms allow entering the nucleus efficiently only in dividing cells, because of nuclear envelope rearrangements naturally occurring at prometaphase. In contrast, Au@DBPs are virus-free delivery vehicles that elicited nuclear envelope reorganization also in non-dividing cells. Hence, Au@DBPs were able to take advantage of these properties, move in the crowded cellular environment and change the permeability of the nucleus compartment.

Targeting of drugs and NPs to tumors poses particular difficulties in delivery; drugs only penetrate few cells around blood vessels [46, 47]. This problem is particularly found in solid tumors, which are poorly perfused because blood vessels and lymphatics are usually dysfunctional. The leakiness of tumor vessels impairs enhanced permeability and retention effect of compounds delivered [48]. The capacity of Au@DBPs to be transferred from one cell to another could boost spreading of therapeutic NPs reaching neighboring cells. This would allow optimal dosage, increasing therapeutic effect and minimizing side effects.

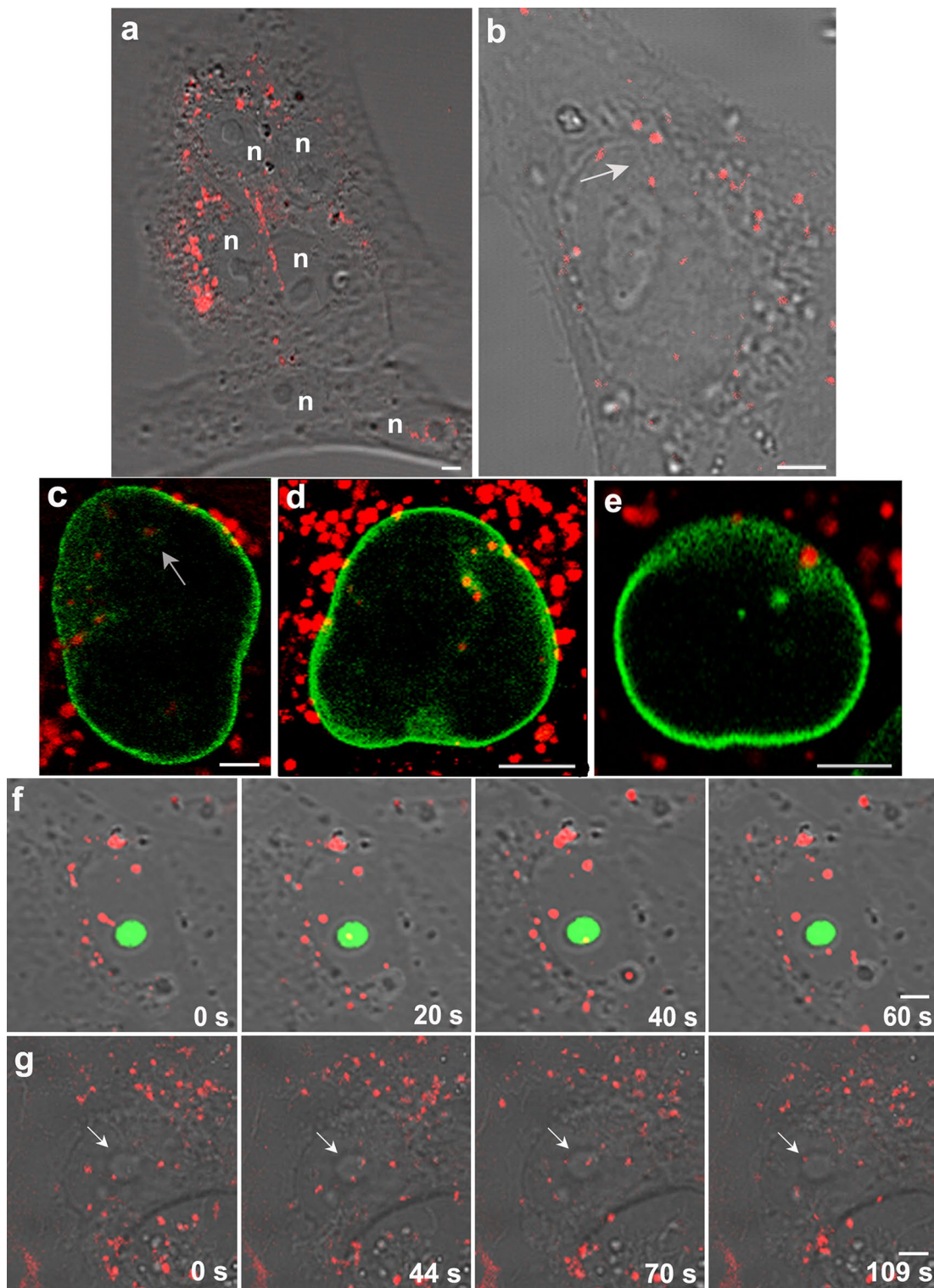


Fig. 5 **a, b** Nuclear penetration capacity of Au@DynPro (n: nucleus). **c–e** Nuclear envelope appeared discontinuous as Au@DynPro shuttle the nucleus in Vero cells transfected with GFP-laminB receptor (**c**) and GFP-laminB1 (**d, e**) as shown in equatorial optical sections. Sample images show NPs entering the nucleus and nuclear lamina folding at sites of NPs entry. **f** Peptides shuttle the nucleus in Vero cells transfected with GFPB23 nucleolin (**g**) Au@DynPro in their way across the nucleus with visible imprints of their paths (**b**, arrow). Scale bar: 5 μ m

Conclusions

We have shown dynein-motor powered NP motility in the crowded cellular environment and across the nuclear envelope. The dynamic properties of these Au@DBPs made them especially appropriate to load compounds and achieve the desired requirements of intracellular delivery to all compartments. Moreover, the quick spreading of these functionalized NPs between cells, remaining intracellular, reduces exposure to the extracellular environment minimizing eventual losses. These characteristics, together with their intracellular accumulation capacity would in turn allow reductions on administration doses of a given drug or therapy because of its better bioavailability in a handful of applications.

Methods

Peptides and cell lines

Peptide sequences spanned the DYNLL1 binding domain of viral proteins (Table 1), that is, African swine fever virus p54 (DynPro) and a shorter sequence including critical amino acids for binding (ShortPro), Rabies virus P protein (TransRb), and control non-dynein-binding amino acid sequence (IntCt). An octa-arginine tail was added to all these peptides, which were also labeled with TAMRA. Peptides were synthesized and purified by HPLC over 95% of purity by Genecust. The following cell lines were tested: Vero kidney epithelial cells (ATCC CCL-81), Madin-Darby Canine Kidney Epithelial Cells (MDCK; ATCC CCL-34), Human embryonic kidney cells transformed with adenovirus 5 (HEK293T/17; ATCC CRL-11268), and Epidermal cancer cells (HeLa; CCL-2). Cells were cultured in DMEM with FBS from Lonza. SK-N-MC human neuroblastoma cells were cultured in EMEM with pyruvate (ATCC HTB-10). These mammalian cells were incubated in sterile 35-mm culture dishes with 10 μ M peptides, or 1.5 μ M NPs, in a CO₂ incubator at 37 °C for 1 h and then imaged.

Chemicals for nanoparticle synthesis

All the chemicals were of reagent grade and were used without further purification. Hydrogen tetrachloroaurate (III) trihydrate (99.9%), (N-(3-dimethylaminopropyl)-N'-ethylcarbodiimide hydrochloride, Tris(hydroxymethyl) aminomethane (TRIS, >98.8%) and 2-[N-morpholino] ethanesulfonic acid (99.5%) were purchased from Sigma-Aldrich; N-(2-mercaptopropionyl) glycine (>98%) and N-hydroxysulfosuccinimide (>97%) were purchased from Fluka and NaBH₄ (98%) from Lancaster. Dynein binding peptides (DBPs, *i.e.* DynPro, ShortPro and TransRb) and the control peptide (IntCt) were purchased from Genecust; α -methoxy- ω -amino polyethylene glycol (CH₃O-PEG-NH₂, 750 Da) was obtained from Rapp-Polymer. Tetramethylrhodamine

5-carboxamide cadaverine (TAMRA-CAD) was purchased from Anaspec. Phosphate buffer saline (PBS) was obtained from Lonza. House distilled water was further purified using a Milli-Q reagent grade water system (Millipore). Buffers were prepared according to standard laboratory procedure. Other chemicals were reagent grade and used as received.

Nanoparticle synthesis and characterization

Characterization

UV-Vis spectra were carried out with Varian Cary 50 spectrophotometer. Fluorescence spectra were carried out with a LS-55 Fluorescence Spectrometer. ζ -potential measurements were done using a ZetaPALS analyser from Brookhaven. All spectra were collected in MilliQ water; for ζ -potential characterization the aqueous solution was adjusted to 1 mM KCl. For TEM examinations, a single drop (5 μ l) of the aqueous solution (0.1 mg ml⁻¹) of the Au NPs was placed onto a copper grid coated with a carbon film. The grid was left to dry in air for several hours at room temperature. TEM analysis was carried out on a Tecnai 20 FEI microscope operated at 200 kV. Particle size distribution of the Au NPs was evaluated from several micrographs using a program for image processing and analysis (ImageJ).

Au@tiopronin

Hydrogen tetrachloroaurate(III) trihydrate (0.15 g, 0.4 mmol) and N-(2-mercaptopropionyl) glycine (tiopronin; 0.19 g, 1.2 mmol) were codissolved in 20 ml of 6:1 methanol/acetic acid, giving a ruby red solution. NaBH₄ (0.30 g, 8.0 mmol) in 7.5 ml of H₂O was added with rapid stirring. The black suspension that was formed was stirred for an additional 30 min after cooling, and the solvent was then removed under vacuum at 40 °C. The crude Au@tiopronin was completely insoluble in methanol but quite soluble in water. It was purified by dialysis, in which the pH of 130 mg of crude product dissolved in 20 ml of water was adjusted to 1 by dropwise addition of concentrated HCl. This solution was loaded into 15 cm segments of seamless cellulose ester dialysis membrane (Sigma, MWCO 10 kDa), placed in 4 l beakers of water, and stirred slowly, recharging with fresh water approximately every 10 h over the course of 72 h. The dark blue Au@tiopronin solutions were collected from the dialysis tubes and were lyophilized. Yield: 96 mg.

Au@peptides/TAMRA-CAD/PEG

N-(3-Dimethylaminopropyl)-N'-ethylcarbodiimide hydrochloride (EDC; 1 mg, 5 μ mol) and N-hydroxysulfosuccinimide (sulfo NHS; 3 mg, 13.5 μ mol) were added to 1 ml of Au@tiopronin (1 mg) in 2-[N-morpholino] ethanesulfonic acid (MES) (50 mM, pH 6.5). NPs were left

to react with EDC (carbodiimide activation) over 30 min at 37 °C under mild stirring conditions. NPs were then purified of excess EDC and sulfo NHS) over a PD-10 column (GE Healthcare). The peptide DynPro (27.5 nmol) or ShortPro (27.5 nmol) or TransRb (27.5 nmol) or IntCt3 (27.5 nmol) or TAMRA-CAD (55 nmol) were added and the mixture was stirred over 1 h at room temperature before the addition of CH₃O-PEG-NH₂ (750 Da; 2.6 μmol) for coupling to remaining activated carboxylic groups; then samples were left under mild stirring conditions at 4 °C overnight. Then, this solution was loaded into centrifugal filters (Amicon Ultra-0.5 ml, MWCO 10 kDa) for three consecutive steps of purification of potentially uncoupled peptide, TAMRA or PEG, and concentration of the mixture prior to suspension in water. For preventing the possible absorption (non-covalently attached to the NPs) of TAMRA or any of the peptides, samples (0.5 ml at 2 mg mL⁻¹) were loaded into ca. 1 cm segments of seamless cellulose ester dialysis membrane (Sigma, MWCO 10 kDa), placed in 1 l beakers of a solution 1 M NaCl in MilliQ water, and stirred slowly over the course of 72 h, recharging with fresh saline solution approximately every 10 h. Then, samples were desalted over a PD-10 column, concentrated with centrifugal filters (Amicon Ultra-0.5 ml, MWCO 10 kDa), suspended in PBS (for cell cultures) or water (for characterization) at 2 mg ml⁻¹, and filtrated over 0.22 μm cellulose filters for sterilization. ζ-potential measurements are shown in Additional file 1: Table S1; UV-Vis and fluorescence spectra are shown in Additional file 1: Figures S1 and S2.

Control samples were prepared for all of the peptide types and TAMRA using the same conditions with the exception of EDC and S-NHS, aiming to prove that unspecific absorption of the peptides on the NPs was avoided. These samples were cleaned as the activated samples and they were characterized by UV/Vis and fluorescence spectroscopy, showing the absence of observable unspecific absorption (*i.e.*, lack of fluorescence).

Incubation of cells with nanoparticles

All the experiments were carried out under sterile conditions working with microbiological class II safety cabinets. The NPs were resuspended in H₂O, with a degree of purity milliQ and sterile, to obtain stock solutions at different concentrations. Special attention was paid to avoid turbidity in the solution and tips were always used with a filter to avoid possible cross contaminations. 500 μl aliquots were stored at 4 °C until the time of use. Working solutions of the NPs were made from stock solutions in DMEM SC medium (10% Foetal bovine serum (FBS), 1% penicillin/streptomycin (PS), 1% Glutamine (G)) and adjusted to 0.2 mg/ml (1.5 μM NPs). The maximum number of NPs used per cell was estimated to be

2.7×10^9 NPs/cell, that is, 300 μl of a solution of 1.5 μM NPs that was added to 10⁵ cells. In order to perform in vitro assays, Vero cells were cultured in 35 mm glass plates overnight. The cells were washed in DMEM SC (10% FBS, 1% PS, 1% G) and the existing medium was replaced by 300 ml of the solutions containing the NPs at optimal concentration of 1.5 μM. The NPs were incubated in incubation chambers at 37 °C and 5% CO₂ and observed with the confocal microscope. The incubation time periods ranged from 20 min to 3 h to observe different degree of accumulation in the cells.

Plasmids and transfections

A vector encoding enhanced green fluorescent protein (EGFP)-LBR (Lamin B receptor) was kindly provided by Loren Fong from UCLA. Plasmid encoding EGFP-Lamin B1 was a generous gift of Howard Worman from Columbia University New York. EGFP-tubulin and -actin, were from Clontech. A vector encoding B23 nucleolar protein was kindly provided by Carmen Rivas from Centro Nacional de Biotecnología, Madrid.

Transfections were performed by using the TransIT 2020 Transfection Reagent from Mirus according to the manufacturer's recommendations. Briefly, Vero cells were grown on 35 mm tissue culture plates, in DMEM (5% FBS, 1% PS, 1% G), until 80% confluence. Separately, 50 μl of DMEM, serum- and antibiotics-free, was mixed with 0.5 μg of DNA and 1.3 μl of TransIT 2020. The mixture was incubated for 20 min at room temperature before addition to cells. To minimize cytotoxicity and increase the efficiency of the transfection, cells medium was replaced by 300 μl of fresh DMEM 5% serum and antibiotics-free before adding the DNA-TransIT mixture. Similarly, after 4 h, the transfection mixture was removed from cells and 500 μl of fresh medium (5% FBS, 1% PS, 1% G) was added. At 24 h after transfection, cells were incubated with the NPs as explained below and analyzed by confocal microscopy.

Inhibition assays

Nocodazole was used at concentration of 2.5 μM and actin depolymerizing Latrunculin A at 0.1 μM. We first ensured that cytotoxicity, determined by the trypan blue exclusion method, did not exceed 10% of cell death after drug incubation at the indicated working concentrations. Cells were pretreated for 30 min with inhibitors at the indicated working concentrations in growth medium for 30 min at 37 °C, further incubated with 1.5 μM of NPs for 30 min at 37 °C and then imaged. After 2 h, culture medium was replaced and washed for 1 h and then imaged.

Cell viability and proliferation assays

To evaluate cell viability after incubation with peptides and NPs, Vero cells seeded in 24 well plates were incubated in DMEM containing delivery DBP or negative control IntCt at concentrations ranging from 0 to 100 μM of each peptide. For NPs the concentrations were ranging from 0 to 1 mg/ml (1–7.5 μM NPs). After incubation with peptides or nanoparticles for 24 h, cells were harvested and the number of viable cells present in the cell suspensions was determined by Tripa blue dye exclusion assay (Sigma). Briefly, 20 μl of PBS with Tripa Blue 0.08% (w/v) were added to equal volume of cell suspension and mixed. After 2 min, blue cells (dead cells) were counted using a hemacytometer and a conventional light microscope.

To evaluate cell proliferation 3×10^4 Vero cells/well seeded in 96 well plates were incubated in 50 μl DMEM containing DBPs and negative control or NPs at the range of concentrations previously used in the cell viability assays. After 24 h incubation, cell proliferation was determined using CellTiter 96 Aqueous™ (Promega) assay, following manufacturer's indications.

Flow cytometry

Vero cells seeded in 24-well plates were incubated for 120 min at 37 °C with Au@DBPs at several concentrations. Then, cells were washed with PBS, harvested by trypsinization and washed again with flow cytometry buffer (PBS, 0.01% sodium azide and 0.1% bovine serum albumin). In order to determine the fluorescence intensity per dose, 10,000 cells/per each Au@DBPs concentration were scored and analysed in a FACS Canto II flow cytometer (BD Sciences).

Time-lapse video microscopy

Confocal microscopy was carried out using a Leica TCS SPE confocal microscope that included a humidified incubation chamber, a CO₂ controller and a heating unit. Selected stacks were recorded every 10-s using the Leica Microsystems LAS AF program and the films were displayed at 1–5 frames/s.

Fluorescence quantification

To quantify the intracellular accumulation of different DBP, cytoplasmic and background regions were selected and mean fluorescence intensity (MFI) quantified. Final MFI was calculated as indicated (cytoplasmic region—background). Quantitative analysis of MFI was performed with the Leica LAS-AF imaging program. At least thirty cells from three independent experiments were examined for each formulation.

Data analysis

One-way analysis of variance was performed with the statistical package GraphPad InStat. Bonferroni's correction was applied for multiple comparisons. Data were presented as mean standard deviations. Differences were considered statistically significant with a p value of 0.001 ($\alpha = 0.05$).

Additional files

Additional file 1: Figure S1. UV/Vis spectra of “bare” NPs (Au@tiopronin) before the modification, and peptide, PEG or TAMRA-CAD modified NPs. a) DBP (red line, Au@tiopronin-DynPro), IntCT (cyan line, Au@tiopronin-IntCt) and TAMRA (blue line, Au@tiopronin-IntCt-TAMRA-CAD); b) DBP-PEG (red line, Au@tiopronin-DynPro/PEG), IntCT-PEG (cyan line, Au@tiopronin-IntCt/PEG) and TAMRA-PEG (blue line, Au@tiopronin-IntCt-TAMRA-CAD/PEG). **Figure S2.** Fluorescence spectra of “bare” NPs (Au@tiopronin) before the modification, and peptide, PEG or TAMRA-CAD modified NPs. a) DBP (red line, Au@tiopronin-DynPro), IntCT (cyan line, Au@tiopronin-IntCt) and TAMRA (blue line, Au@tiopronin-IntCt-TAMRA-CAD); b) DBP-PEG (red line, Au@tiopronin-DynPro/PEG), IntCT-PEG (cyan line, Au@tiopronin-IntCt/PEG) and TAMRA-PEG (blue line, Au@tiopronin-IntCt-TAMRA-CAD/PEG). **Figure S3.** ζ -potential bar diagram of “bare” NPs (Au@tiopronin) before the modification, and modified peptide or TAMRA-CAD modified NPs: DBP (Au@DynPro), IntCT (Au@IntCt), TAMRA (Au@TAMRA-CAD), DBP-PEG (Au@DynPro/PEG), IntCT-PEG (Au@IntCt/PEG) and TAMRA-PEG (Au@TAMRA-CAD/PEG). **Table S1.** ζ -potential values of “bare” NPs (Au@tiopronin) before the modification, and peptide, PEG or TAMRA-CAD modified NPs: DBP (Au@DynPro), IntCT (Au@IntCt), TAMRA (Au@TAMRA-CAD), DBP-PEG (Au@DynPro/PEG), IntCT-PEG (Au@IntCt/PEG) and TAMRA-PEG (Au@TAMRA-CAD/PEG). **Figure S4.** The figure shows the cellular uptake (according to intracellular MFI) of Au@DynPro, Au@DynPro-PEG, compared to nanoparticles modified with internal control peptide (IntCt), Au@IntCt and Au@IntCt-PEG. Mean fluorescence intensity (MFI) of modified NPs after 1 h incubation. **Figure S5.** This figure shows the absence of cytotoxic effect of the NPs in Vero cells. Cell viability (a) and cell proliferation (b) were analyzed after incubation of cells with increasing concentrations of the different Au@DBP that exceeded those used in this study. A significant decrease in cell counts or cell proliferation was not observed.

Additional file 2: Movie 1. Motion beyond cell boundaries. This movie shows a general view of Au@DBP motion and dispersion in 293T cells incubated with 0.2 mg/ml of Au@DynPro during 1.5 h. Au@DBP displayed short and long tracks of bidirectional motion along a cell projection connecting a neighboring cell. Movement results in transfer of Au@DynPro to the latter. The time lapse covers about 7 min at a rate of 5 frames/s.

Additional file 3: Movie 2. Intracellular movement of NPs linear trajectories. This movie displays a Vero cell incubated with Au@DynPro at 0.2 mg/ml during 1.5 h showing linear and stable tracks of directed motion in the perinuclear area. The time lapse covers 40 s at a rate of 3 frames/s.

Authors' contributions

ID, PdP, JMF and CA designed the research plan and experiments. ID, PdP, BP, MAC-G, IG and MM carried out the experiments. ID, PdP, JMF and CA wrote the manuscript. All authors read and approved the final manuscript.

Author details

¹ Dpt. Biotecnología, Instituto Nacional de Investigación y Tecnología Agraria y Alimentaria (INIA), Carretera de la Coruña km 7.5, 28040 Madrid, Spain. ² Instituto de Nanociencia de Aragón, Universidad de Zaragoza, Mariano Esquillor, s/n, 50018 Zaragoza, Spain. ³ Centro Singular de Investigación en Química Biológica e Materiais Moleculares (CiQUS), Departamento de Física de Partículas, Universidad de Santiago de Compostela, 15782 Santiago de Compostela, Spain. ⁴ Aragon Materials Science Institute (ICMA), CSIC-University of Zaragoza and CIBER-BBN, C/Pedro Cerbuna 12, 50009 Zaragoza, Spain.

Acknowledgements

We thank H. Worman from Columbia University for EGFP-LaminB1, L. Fong from UCLA for the EGFP-Lamin B receptor and C. Rivas at CNB-UAM, Madrid for the EGFP-B23 nucleolar protein. We also thank P. Lammerding, Y. Hernández and V. Grazú for suggestions. The authors thank I. Echaniz and S. Rivera for technical assistance.

Competing interests

The authors declare that they have no competing interests.

Availability of data and materials

All data generated or analyzed during this study are included in this published article (and its additional files).

Consent for publication

All authors read and approved the final manuscript.

Ethics approval and consent to participate

Not applicable.

Funding

The present work was supported by grants from the Spanish Ministry of Economy, Industry and Competitiveness AGL2012-34533, AGL2015-69598-R, SAF2014-54763-C2-2-R, Fondo Social de la DGA (grupos DGA), ERC-Starting Grant 239931-NANOPUZZLE and COST Action CA15138 Transautophagy. PdP and BP thanks financial support from the Consellería de Cultura, Educación e Ordenación Universitaria (Centro singular de investigación de Galicia accreditation 2016–2019, ED431G/09), and the European Regional Development Fund (ERDF).

Publisher's Note

Springer Nature remains neutral with regard to jurisdictional claims in published maps and institutional affiliations.

Received: 22 December 2017 Accepted: 19 March 2018

Published online: 30 March 2018

References

- Hess H. Engineering applications of biomolecular motors. *Annu Rev Biomed Eng.* 2011;13:429–50.
- Kolomeisky AB. Motor proteins and molecular motors: how to operate machines at the nanoscale. *J Phys Condens Matter.* 2013;25:463101.
- Falanga A, Vitiello MT, Cantisani M, Tarallo R, Guarnieri D, Mignogna E, et al. A peptide derived from herpes simplex virus type 1 glycoprotein H: membrane translocation and applications to the delivery of quantum dots. *Nanomedicine.* 2011;7:925–34.
- Moros M, Hernaez B, Garett E, Dias JT, Saez B, Grazu V, et al. Monosaccharides versus PEG-functionalized NPs: influence in the cellular uptake. *ACS Nano.* 2012;6:1565–77.
- Bareford LM, Swaan PW. Endocytic mechanisms for targeted drug delivery. *Adv Drug Deliv Rev.* 2007;59:748–58.
- dos Santos T, Varela J, Lynch I, Salvati A, Dawson KA. Effects of transport inhibitors on the cellular uptake of carboxylated polystyrene nanoparticles in different cell lines. *PLoS One.* 2011;6:e24438.
- Hess H, Vogel V. Molecular shuttles based on motor proteins: active transport in synthetic environments. *J Biotechnol.* 2001;82:67–85.
- Ruenraroengsak P, Florence AT. Biphasic interactions between a cationic dendrimer and actin. *J Drug Target.* 2010;18:803–11.
- Ng CP, Goodman TT, Park IK, Pun SH. Bio-mimetic surface engineering of plasmid-loaded nanoparticles for active intracellular trafficking by actin comet-tail motility. *Biomaterials.* 2009;30:951–8.
- Barua S, Rege K. The influence of mediators of intracellular trafficking on transgene expression efficacy of polymer-plasmid DNA complexes. *Biomaterials.* 2010;31:5894–902.
- Alonso C, Miskin J, Hernaez B, Fernandez-Zapatero P, Soto L, Canto C, et al. African swine fever virus protein p54 interacts with the microtubular motor complex through direct binding to light-chain dynein. *J Virol.* 2001;75:9819–27.
- Leopold PL, Pfister KK. Viral strategies for intracellular trafficking: motors and microtubules. *Traffic.* 2006;7:516–23.
- Sherer NM, Lehmann MJ, Jimenez-Soto LF, Horensavitz C, Pypaert M, Mothes W. Retroviruses can establish filopodial bridges for efficient cell-to-cell transmission. *Nat Cell Biol.* 2007;9:310–5.
- Smith GA, Enquist LW. Break ins and break outs: viral interactions with the cytoskeleton of Mammalian cells. *Annu Rev Cell Dev Biol.* 2002;18:135–61.
- Kawashima D, Kanda T, Murata T, Saito S, Sugimoto A, Narita Y, et al. Nuclear transport of Epstein-Barr virus DNA polymerase is dependent on the BMRF1 polymerase processivity factor and molecular chaperone Hsp90. *J Virol.* 2013;87:6482–91.
- Dodding MP, Way M. Coupling viruses to dynein and kinesin-1. *EMBO J.* 2011;30:3527–39.
- Kelkar SA, Pfister KK, Crystal RG, Leopold PL. Cytoplasmic dynein mediates adenovirus binding to microtubules. *J Virol.* 2004;78:10122–32.
- Xiao PJ, Samulski RJ. Cytoplasmic trafficking, endosomal escape, and perinuclear accumulation of adeno-associated virus type 2 particles are facilitated by microtubule network. *J Virol.* 2012;86:10462–73.
- Kardon JR, Vale RD. Regulators of the cytoplasmic dynein motor. *Nat Rev Mol Cell Biol.* 2009;10:854–65.
- Karki S, Holzbaur EL. Cytoplasmic dynein and dynactin in cell division and intracellular transport. *Curr Opin Cell Biol.* 1999;11:45–53.
- Carter AP. Crystal clear insights into how the dynein motor moves. *J Cell Sci.* 2013;126:705–13.
- Raaijmakers JA, Tanenbaum ME, Medema RH. Systematic dissection of dynein regulators in mitosis. *J Cell Biol.* 2013;201:201–15.
- Salina D, Bodoor K, Eckley DM, Schroer TA, Rattner JB, Burke B. Cytoplasmic dynein as a facilitator of nuclear envelope breakdown. *Cell.* 2002;108:97–107.
- Beaudouin J, Gerlich D, Daigle N, Eils R, Ellenberg J. Nuclear envelope breakdown proceeds by microtubule-induced tearing of the lamina. *Cell.* 2002;108:83–96.
- Shekhar N, Wu J, Dickinson RB, Lele TP. Cytoplasmic dynein: tension generation on microtubules and the nucleus. *Cell Mol Bioeng.* 2013;6:74–81.
- Kutay U, Hetzer MW. Reorganization of the nuclear envelope during open mitosis. *Curr Opin Cell Biol.* 2008;20:669–77.
- Siglin AE, Sun S, Moore JK, Tan S, Poenie M, Lear JD, et al. Dynein and dynactin leverage their bivalent character to form a high-affinity interaction. *PLoS One.* 2013;8:e59453.
- Pfister KK, Fisher EM, Gibbons IR, Hays TS, Holzbaur EL, McIntosh JR, et al. Cytoplasmic dynein nomenclature. *J Cell Biol.* 2005;171:411–3.
- Schroer TA. Dynactin. *Annu Rev Cell Dev Biol.* 2004;20:759–79.
- Martinez-Moreno M, Navarro-Lerida I, Roncal F, Albar JP, Alonso C, Gavilanes F, et al. Recognition of novel viral sequences that associate with the dynein light chain LC8 identified through a pepscan technique. *FEBS Lett.* 2003;544:262–7.
- Hernaez B, Tarrago T, Giralte E, Escibano JM, Alonso C. Small peptide inhibitors disrupt a high-affinity interaction between cytoplasmic dynein and a viral cargo protein. *J Virol.* 2010;84:10792–801.
- Radnai L, Rapali P, Hodi Z, Suveges D, Molnar T, Kiss B, et al. Affinity, avidity, and kinetics of target sequence binding to LC8 dynein light chain isoforms. *J Biol Chem.* 2010;285:38649–57.
- Pelaz B, Charron G, Pfeiffer C, Zhao Y, de la Fuente JM, Liang XJ, et al. Interfacing engineered nanoparticles with biological systems: anticipating adverse nano-bio interactions. *Small.* 2012;9:1573–84.
- Templeton AC, Wuelfing WP, Murray RW. Monolayer-protected cluster molecules. *Acc Chem Res.* 2000;33:27–36.
- de la Fuente JM, Berry CC, Riehle MO, Curtis AS. Nanoparticle targeting at cells. *Langmuir.* 2006;22:3286–93.
- Romberg B, Hennink WE, Storm G. Sheddable coatings for long-circulating nanoparticles. *Pharm Res.* 2008;25:55–71.
- del Pino P, Yang F, Pelaz B, Zhang Q, Kantner K, Hartmann R, et al. Basic physicochemical properties of polyethylene glycol coated gold nanoparticles that determine their interaction with cells. *Angew Chem Int Ed.* 2016;55:5483–7.
- Pelaz B, del Pino P, Maffre P, Hartmann R, Gallego M, Rivera-Fernandez S, et al. Surface functionalization of nanoparticles with polyethylene glycol: effects on protein adsorption and cellular uptake. *ACS Nano.* 2015;9:6996–7008.

39. Raux H, Flamand A, Blondel D. Interaction of the rabies virus P protein with the LC8 dynein light chain. *J Virol*. 2000;74:10212–6.
40. Urnavicius L, Zhang K, Diamant AG, Motz C, Schlager MA, Yu M, et al. The structure of the dynactin complex and its interaction with dynein. *Science*. 2015;347:1441–6.
41. Parassol N, Bienvenu C, Boglio C, Fiorucci S, Cerezo D, Yu X-M, et al. In vivo characterization of dynein-driven nanovectors using *Drosophila* oocytes. *PLoS One*. 2013;8:e82908.
42. Akita H, Enoto K, Tanaka H, Harashima H. Particle tracking analysis for the intracellular trafficking of nanoparticles modified with African swine fever virus protein p54-derived peptide. *Mol Ther*. 2013;21:309–17.
43. Cohen O, Granek R. Nucleus-Targeted Drug Delivery: Theoretical Optimization of Nanoparticles Decoration for Enhanced Intracellular Active Transport. *Nano Lett*. 2014;14:2515–21.
44. Fytianos K, Chortarea S, Rodriguez-Lorenzo L, Blank F, von Garnier C, Petri-Fink A, et al. Aerosol delivery of functionalized gold nanoparticles target and activate dendritic cells in a 3D lung cellular model. *ACS Nano*. 2017;11:375–83.
45. Tiwari G, Tiwari R, Sriwastawa B, Bhati L, Pandey S, Pandey P, et al. Drug delivery systems: an updated review. *Int J Pharm Investig*. 2012;2:2–11.
46. Hait WN, Hambley TW. Targeted cancer therapeutics. *Cancer Res*. 2009;69:1263–7 (**discussion 7**).
47. Iyer AK, Khaled G, Fang J, Maeda H. Exploiting the enhanced permeability and retention effect for tumor targeting. *Drug Discov Today*. 2006;11:812–8.
48. Sugahara KN, Teesalu T, Karmali PP, Kotamraju VR, Agemy L, Girard OM, et al. Tissue-penetrating delivery of compounds and nanoparticles into tumors. *Cancer Cell*. 2009;16:510–20.

Submit your next manuscript to BioMed Central and we will help you at every step:

- We accept pre-submission inquiries
- Our selector tool helps you to find the most relevant journal
- We provide round the clock customer support
- Convenient online submission
- Thorough peer review
- Inclusion in PubMed and all major indexing services
- Maximum visibility for your research

Submit your manuscript at
www.biomedcentral.com/submit

